Published in final edited form as:
Free Radic Biol Med. 2012 August 15; 53(4): 951–961. doi:10.1016/j.freeradbiomed.2012.06.003.

Desferrioxamine Inhibits Protein Tyrosine Nitration: Mechanisms and Implications

Margaret A. Adgent[1,3], **Giuseppe L. Squadrito**[1,3], **Carol A. Ballinger**[1,3], **David M. Krzywanski**[1,3], **Jack R. Lancaster**[2,3], and **Edward M. Postlethwait**[1,3]

[1]Department of Environmental Health Sciences School of Public Health, University of Alabama at Birmingham Birmingham, Alabama

[2]Department of Anesthesiology Department of Physiology & Biophysics School of Medicine, University of Alabama at Birmingham Birmingham, Alabama

[3]Center for Free Radical Biology, University of Alabama at Birmingham Birmingham, Alabama

Abstract

Tissues are exposed to exogenous and endogenous nitrogen dioxide ($^{\bullet}NO_2$), which is the terminal agent in protein tyrosine nitration. Besides iron chelation, the hydroxamic acid (HA) desferrioxamine (DFO) shows multiple functionalities including nitration inhibition. To investigate mechanisms whereby DFO affects 3-nitrotyrosine (3-NT) formation, we utilized gas phase $^{\bullet}NO_2$ exposures, to limit introduction of other reactive species, and a lung surface model wherein red cell membranes (RCM) were immobilized under a defined aqueous film. When RCM were exposed to $^{\bullet}NO_2$ covered by +/− DFO: (i) DFO inhibited 3-NT formation more effectively than other HA and non-HA chelators; (ii) 3-NT inhibition occurred at very low [DFO] for prolonged times; and (iii) 3-NT formation was iron independent but inhibition required DFO present. DFO poorly reacted with $^{\bullet}NO_2$ compared to ascorbate, assessed via $^{\bullet}NO_2$ reactive absorption and aqueous phase oxidation rates, yet limited 3-NT formation at far lower concentrations. DFO also inhibited nitration under aqueous bulk phase conditions, and inhibited 3-NT generated by active myeloperoxidase “bound” to RCM. Per the above and kinetic analyses suggesting preferential DFO versus $^{\bullet}NO_2$ reaction within membranes, we conclude that DFO inhibits 3-NT formation predominantly by facile repair of the tyrosyl radical intermediate, which prevents $^{\bullet}NO_2$ addition, and thus nitration, and potentially influences biochemical functionalities.

Keywords

Desferrioxamine; nitrogen dioxide; membrane proteins; hydroxamic acids; epithelial lining fluid; nitration; tyrosine; tyrosyl radicals; repair; reduction

Correspondence to: Edward M. Postlethwait, Ph.D., Department of Environmental Health Sciences, University of Alabama at Birmingham, RPHB 530, 1530 3rd Avenue South Birmingham, AL 35294-0022, Office: (205) 934-7085, FAX: (205) 975-6341, epost@uab.edu.

Introduction

Desferrioxamine (DFO), a siderophore produced by *Streptomyces pilosus,* is currently the most widely employed iron chelator and is administered clinically to promote the excretion of toxic iron. It consists of a chain of three hydroxamic acids (see Fig. 1) which allows it to bind ferric (Fe^{3+}) iron with a stability constant of 10^{31} [1]. Apart from its clinical use, DFO is useful in investigating free-radical induced injury [2]. DFO reacts with both superoxide and hydroxyl radicals, affects eicosanoid metabolism, acts as a substrate for peroxidases and inhibits them at high concentrations, and is capable of forming a nitroxide radical [3,4]. In animal studies, DFO has shown protective effects on $^{\bullet}NO_2$- and smoke-induced lung injury [5,6]. These effects have been almost entirely attributed to iron chelation and thus inhibition of iron-dependant free radical reactions. However, it has also been proposed that DFO can inhibit free radical reactions by iron chelation-independent mechanisms such as direct scavenging of reactive species including the nitrogen dioxide radical ($^{\bullet}NO_2$) [7–9].

It is widely believed that $^{\bullet}NO_2$ is pivotal in biological nitration reactions [10–13], that have been observed concomitant with a variety of pathophysiologic conditions [14–17]. In vivo exposure to $^{\bullet}NO_2$ occurs via direct inhalation, decomposition of higher order nitrogen oxides, peroxidase-mediated reactions, $^{\bullet}NO$ near diffusion-controlled reaction with organic peroxyl radicals which form $^{\bullet}NO_2$ and the corresponding alkoxyl radicals, and, to a limited extent, autoxidation of nitric oxide ($^{\bullet}NO$) [11–13,18–21]. The reaction of peroxynitrite with CO_2, that ultimately forms the $^{\bullet}NO_2$ and $CO_3^{\bullet-}$ radicals, and $^{\bullet}NO_2$ catalytically generated by the enzyme myeloperoxidase using nitrite as a substrate, are commonly associated with the nitration of tyrosine residues. However, these reactions may not be the sole sources of $^{\bullet}NO_2$, especially in the outermost tissue strata. The lung, for example, endogenously generates $^{\bullet}NO$ and is frequently exposed to environmental $^{\bullet}NO$ and $^{\bullet}NO_2$ that can be absorbed from the intrapulmonary gas phase by diffusive and reactive processes [18,20,22,23]. Within the lung, in a concentration dependent manner, $^{\bullet}NO_2$ exposure initiates acute epithelial injury, activation of signaling cascades, inflammation, protein and lipid oxidation, and, ultimately remodeling of lung architecture [18,24–26].

The entire respiratory tract surface is covered by a biochemically complex aqueous layer termed the epithelial lining fluid (ELF) into which inhaled gases dissolve and then must diffuse before contacting the underlying epithelia. Reactive absorption, wherein ELF reactions with solute $^{\bullet}NO_2$ maintain the net driving force for continued mass transfer of $^{\bullet}NO_2$ from the gas to aqueous phase [22,27,28], may play an important role in lung surface compartment nitration. Because $^{\bullet}NO_2$ undergoes facile reaction with numerous ELF constituents and because recent comprehensive analyses suggest markedly reduced hydrophobic partitioning relative to $^{\bullet}NO$ [21,29,30], initial $^{\bullet}NO_2$ reactions are likely largely confined to the ELF. Thus, depending upon the respective concentrations of $^{\bullet}NO_2$ and ELF substrates and the ELF thickness, diffusion versus reaction properties will dictate how far $^{\bullet}NO_2$ penetrates into and through the ELF, which varies in thickness from 1 to 10 μm [31]. Recent estimates suggest that $^{\bullet}NO_2$ reaction with ELF constituents would predominate over its diffusion to the epithelial surface [21,32].

This is further supported by observations that $^{\bullet}NO_2$ exposure-mediated 3-nitrotyrosine (3-NT) formation occurred in cell membranes when overlain by phosphate buffer but not at appreciable antioxidant concentrations [32]. In addition, inclusion of metal chelators DFO or diethylenetriaminepenta-acetic acid (DTPA) to the model system inhibited exposure-mediated membrane oxidation but, DFO also inhibited membrane nitration while DTPA did not [32,33]. Because tyrosine nitration is generally considered to involve a two step process wherein oxidation generates a tyrosyl radical intermediate followed by $^{\bullet}NO_2$ addition, diverse oxidants other than $^{\bullet}NO_2$ (e.g., carbonate radical, lipid radicals, etc) may contribute

to the first step [12,34]. Consequently, interventions that reduce the extent of tyrosine nitration may result from a variety of mechanisms.

Accordingly, we extended our previous observations of $^{\bullet}NO_2$ reaction/diffusion phenomena via studies to discern mechanisms by which DFO inhibits protein nitration under conditions that approximate the lung surface. A previously utilized reductionist model was employed to facilitate tight experimental controls, including the direct use of gaseous $^{\bullet}NO_2$ which circumvents initial generation of other reactive species that occurs during use of precursor reagents, pulse radiolysis, or flash photolysis [7,12,32–35]. Our results suggest that, in addition to modest direct $^{\bullet}NO_2$ scavenging, DFO reduces tyrosyl radicals and thus inhibits the radical-radical addition step that leads to 3-NT formation.

Materials and Methods

Reagents

Reagents were obtained from the following suppliers: **(i)**compressed $^{\bullet}NO_2$ (99.1 ppm in N_2) - BOC Gases (Riverton, NJ, USA); **(ii)** nitrotyrosine polyclonal antibody, nitrotyrosine BSA, and 3-nitrotyrosine (3-NT) - Cayman Chemical (Ann Arbor, MI, USA); **(iii)** acrylamide, lysine, Tris, nitrocellulose membrane paper and broad range SDS-page - Bio-Rad (Hercules, CA, USA); **(iv)** sodium lauryl sulfate, monobasic and dibasic sodium phosphate - Fisher Scientific (Fair Lawn, NJ, USA); **(v)** SuperSignal west pico chemiluminescent substrate and BCA protein assay kit - Pierce Biotechnology, Inc. (Rockford, IL, USA); **(vi)** L-tyrosine - ICN Biochemical (Cleveland, OH, USA); **(vii)** hydroxyurea (HU) - Calbiochem (La Jolla, CA, USA); **(viii)** N,N′-Di(2-hydroxybenzyl)ethylenediamine-N, N′-diacetic acid monohydrochloride hydrate (HBED) - Strem Chemicals (Newbury Port, MA, USA); **(ix)** desferrioxamine (DFO), salicylhydroxamic acid (SHA), benzohydroxamic acid (BHA), diethylenetriaminepentaacetic acid (DTPA), ascorbic acid (AH_2), ferric chloride ($FeCl_3$), monoclonal anti-rabbit IgG and all other materials - Sigma-Aldrich CO (St. Louis, MO, USA). Structures of the various hydroxamic acids and related reagents are presented in Figure 1. Because of the functional group structural similarities, we shall consider hydroxyurea as a hydroxamic acid.

In vitro lung surface model

Human blood was obtained by venipuncture according to the University of Alabama, Birmingham IRB protocol number X030320005. The lung surface model, as described in [24, 34] was designed to mimic the lung surface via its three compartments; air space, epithelial lining fluid (ELF), and epithelium. Herein, a monolayer of red blood cell-derived membranes (red cell membranes; RCM) bound to the bottom of Petri dishes (60 × 15 mm) represents the epithelial apical surface. Prior to application of red cells, dishes were boiled in 10% nitric acid, silanized with 3-aminopropyltriethoxysilane, and treated with glutaraldehyde to generate a surface of reactive aldehydes capable of binding to the amino termini and other amino moieties of proteins [32,33]. Erythrocytes were washed three times with 310 mOsm phosphate buffer, pH 7.4, and centrifuged at 4000 RCF. 2.3 ml of a 10% erythrocyte suspension (in 310 mOsm phosphate buffer) was added to the dishes and allowed to bind for 30 minutes. The bound cells were then lysed with 2 ml hypotonic phosphate buffer (10 mOsm, pH 7.0), and repeatedly rinsed to remove hemoglobin and other intracellular debris, resulting in a monolayer of RCM covalently bound to the glass surface of the dishes. Immediately prior to exposure, 2 ml model ELF (10 mOsm phosphate buffer + dissolved reagents, pH 7.0 [36]) were added over the RCM. A hypo-osmolar buffer was used during exposure to inhibit RCM re-annealing, which would generate a fourth (intracellular) compartment, leaving a sheet of open membranes so that both “inner” and “outer” sides were exposed to aqueous phase solutes. Reagents included AH_2, $FeCl_3$, iron

chelators DFO, DTPA, HBED, SHA, BHA, and HU. In order to facilitate iron removal prior to exposure initiation, several experiments were conducted wherein either 50 μM DFO or 400 μM DTPA were added to the membranes for 10 minutes followed by repeated rinsing and addition of the model ELF. Ferrioxamine was formed by combining DFO with a molar excess of $FeCl_3$ prior to introduction into the RCM model.

RCM exposure protocol

Petri dishes with bound RCM were exposed to $^{\bullet}NO_2$ for 30 minutes in a small glass chamber (1500 ml). In order to mimic ELF *in situ* thickness, the chamber was intermittently tilted to leave an aqueous film covering the upper half of the dish, which provided a reservoir of reactive substrates pooled in the lower half of the dish. Every two minutes, the chamber was tilted to the opposite angle allowing for each half to be exposed equally [32,33]. Exposures were conducted under steady state, first order conditions with respect to $^{\bullet}NO_2$ [37] ($[^{\bullet}NO_2]_{inflow}$ ~ 4.5 ppm) at 25°C. High concentration $^{\bullet}NO_2$ (~ 100 ppm $^{\bullet}NO_2$ in N_2) was injected countercurrent into a stream of humidified air which then flowed through a diffuser located in the top of the exposure chamber [32], resulting in well-mixed, gas phase conditions (~ 1 volume change/min). To reduce background $^{\bullet}NO_2$ interactions with chamber components, the entire exposure system was equilibrated (wherein $[^{\bullet}NO_2]_{inlet} = [^{\bullet}NO_2]_{outlet}$) prior to Petri dish introduction. Gas phase $^{\bullet}NO_2$ concentrations were continuously monitored via chemiluminescence (Model 42C $^{\bullet}NO_x$ analyzer; Thermo Fisher, Franklin, MA, USA). $^{\bullet}NO$ concentrations were consistently well below 0.10 ppm.

Myeloperoxidase studies

To directly generate $^{\bullet}NO_2$ at the RCM, thus avoiding $^{\bullet}NO_2$ mass transfer into and reaction/diffusion within the overlying aqueous film, RCM were overlain with a 0.7 units/ml MPO solution, the Petri dishes covered, and gently but continuously rocked for 15 min. The MPO solution was then aspirated and the dishes rinsed, resulting in catalytically active MPO adhered to the RCM. MPO activity was assessed via intra-dish reaction mixtures using tetramethylbenzidine as the substrate [38]. Residual (bound) MPO activity averaged 0.56 units/ml, with little inter-dish variation. For nitration studies, RCM + MPO were overlain with various aqueous systems (+/− 100 μM NO_2^- and/or 100 μM H_2O_2) and continuously rocked in covered dishes for 30 min. Following treatment, membrane proteins were isolated and the presence of 3-NT determined by Western analysis.

Flask exposures

50 ml Erlenmeyer flasks were equipped with Teflon covered stoppers, Teflon inlet and exhaust tubes, and stir bars. $^{\bullet}NO_2$ gas phase mixtures were generated as above and the exposure system and flask conditioned until inlet (~ 150 ml/min) and exhaust $[^{\bullet}NO_2]$ were equivalent. Test solutions were directly injected into the flask, exposures conducted under first-order conditions with respect to $[^{\bullet}NO_2]$ and both gas and aqueous phase well stirred conditions, and the time-dependent change in $^{\bullet}NO_2$ exit concentration monitored. This approach permits mass balance computations (i.e. $([^{\bullet}NO_2]_{in} - [^{\bullet}NO_2]_{out}$ x time x flow = total uptake) of $^{\bullet}NO_2$ reactive absorption. Although this is a lumped measure that includes interfacial transfer, $^{\bullet}NO_2$ solubility, both solute $^{\bullet}NO_2$ and reactive substrate diffusion, and bimolecular reaction kinetics, $^{\bullet}NO_2$ uptake (gas phase disappearance) serves as a measure of relative reactivity since, under fixed conditions of $[^{\bullet}NO_2]_{inflow}$, temperature, flow, and stirring, interfacial transfer (uptake) is determined by solute $^{\bullet}NO_2$ reaction which is a function of substrate concentration and reaction rate (k • [S]) [22,30]. NO_2^- accumulation in the model ELF was measured using the Griess reaction [39]. Larger flasks (250 ml) and volumes (20 ml) were also used to assess differential rates of AH_2 and DFO oxidation due to $^{\bullet}NO_2$ exposure. Oxidation was evaluated spectrophotometrically using extinction coefficients (AH_2; $\varepsilon_{(265\ nm)}$ = 14,500 $M^{-1}cm^{-1}$ [40]) and the loss of ability to form

ferrioxamine ($\varepsilon_{(425\ nm)}$ = 2,460 $M^{-1}cm^{-1}$ [41]) in the presence of excess ferric ions (see supplemental data).

Bubbler exposures

Using a fine fritted bubbler equipped with a stopcock at the bottom to allow for sample removal, approximately 8 ppm $^{\bullet}NO_2$ in humidified air, generated as above, was bubbled through a solution of 0.8 mM tyrosine with or without 50 μM DFO (in 10 mOsm phosphate buffer, pH 7.0) for 120 minutes to assess the formation of 3-NT under aqueous bulk phase conditions. Every 30 minutes, 2.25 ml of the exposed solution were combined with 0.25 ml of 1 N NaOH and scanned from 200–800 nm (Cary 100 Bio UV-Visible Spectrophotometer, Walnut Creek, CA, USA). 3-NT displays a broad peak at approximately 430 nm [42].

Western blot analysis of 3-nitrotyrosine formation

RCM nitration was evaluated by Western blot analysis of 3-NT formation in membrane proteins relative to aqueous phase conditions (*e.g.,* AH_2, DTPA, HBED, DFO, DFO + $FeCl_3$, SHA, BHA, HU), and pretreatment conditions (DFO, DTPA). Immediately after exposure, the aqueous phase was removed and RCM were rinsed with phosphate buffer and 150 μl of extraction buffer (150 mM NaCl, 50 mM Tris, 1 mM EGTA, .25% Sodium deoxycholate, 1% Igepal, 1 mM Na orthovanadate, 1 mM protease inhibitor, and 0.4% HCl) was added to each dish to solubilize membrane proteins. The dishes were scraped and the composite extract stored in sealed microfuge tubes (−80°C). Using the BCA assay to determine appropriate loading amounts, 10 μg protein from each sample and nitrated bovine serum albumin (positive control) were separated by gel electrophoresis (10% gel, 50 V, overnight) and transferred to nitrocellulose membranes (25 V, 1 hr) for Western blot analysis. After transfer, blots were stained in fast green to visualize proteins, then blocked in a 5% nonfat milk/TBST (200 mM Tris, 1.5 M NaCl, and 0.05% Tween 20) solution for 1 hr. Blots were rinsed with TBST and incubated in 1:500 nitrotyrosine polyclonal antibody for 1 hr followed by a 1:2500 monoclonal anti-rabbit IgG for an additional 1 hr incubation. The presence of 3-NT was detected with Pierce SuperSignal west pico chemiluminescent substrate.

Data analyses

Because of the high density staining of the 3-NT Western blots, densitometry was impractical for quantification [43,44] and thus we utilized a comparative system wherein each blot was run with an experiment-specific PO_4 + NO_2 positive control, and the resulting extent of 3-NT subjectively scaled. Lanes containing the experimental conditions were evaluated in comparison to the experiment- and blot-specific control lanes, denoting the amount of 3-NT as extensive (++++), significant (+++), modest (++), little (+), or none (−). Each blot was scored by blinded observation. Data represent means +/− standard deviations. Statistical analyses generally employed ANOVA with significance set at $p < 0.05$.

Results

Previous $^{\bullet}NO_2$ reaction/diffusion studies, which employed the same lung surface model herein, noted that protein nitration was ablated when RCM were covered by an aqueous film containing DFO but not DTPA [32], but the mechanism remained equivocal. To elucidate mechanisms for the selective inhibition by DFO, we initially investigated the concentration profile of DFO-related 3-NT inhibition to determine a [DFO] efficacy threshold under these experimental conditions. RCM were exposed (30 min, 4.5 ppm $^{\bullet}NO_2$ in air) using only DFO in buffer and protein nitration evaluated. Concentrations as low as 0.5 μM DFO appreciably decreased exposure-mediated nitration (Fig. 2), suggesting that only small concentrations

were required despite the fact that some DFO reaction with solute $^{\bullet}NO_2$ would potentially occur [7].

We subsequently characterized the temporal course of DFO-mediated nitration inhibition using a [DFO] above that shown to be efficacious for a 30 minute exposure period. Figure 3 illustrates that an initial aqueous phase concentration of 25 μM DFO limited RCM 3-NT formation to near or below detectable levels for at least 90 min of continuous $^{\bullet}NO_2$ exposure. If one considers the mass balance between $^{\bullet}NO_2$ delivery and the DFO pool, approximately 20 μmoles of $^{\bullet}NO_2$ were delivered to the chamber over the 90 min time span (4.5 ppm = 8.46 ng/ml; (8.46 ng/ml • 1200 ml/min • 90 min)/46 ~ 20 μmole). Each RCM dish initially contained 50 nmole DFO so that even with 6 dishes concomitantly exposed (2 ml/dish • 6 dishes = 0.3 μmoles DFO), there was at least a 60-fold excess of $^{\bullet}NO_2$ available for mass transfer and reaction, although $[^{\bullet}NO_2]_{exit}$ indicated somewhat modest $^{\bullet}NO_2$ gas phase disappearance throughout the 90 min exposure period, consistent with limited aqueous substrate reaction [30]. Thus, the prolonged inhibition of protein nitration suggests that pathway(s) other than direct DFO scavenging of solute $^{\bullet}NO_2$ likely predominated.

As a basis for direct comparison of aqueous phase reactants, 3-NT formation was assessed using a well-documented facile $^{\bullet}NO_2$ reactive substrate [29,30]. RCM were exposed (30 min; 4.5 ppm $^{\bullet}NO_2$) while covered with initial AH_2 concentrations ranging from 10 to 100 μM. As shown in Table 1, a pronounced concentration effect was observed wherein only 100 μM AH_2 substantially limited exposure-induced nitration over 30 min. At the lower initial concentrations (≤ 50 μM), no AH_2 could be detected at the end of the exposure period (data not shown). Thus, the differential extent of 3-NT formation across $[AH_2]$ was likely related to reactive absorption-mediated depletion of AH_2, so that the temporal course of protein nitration was a function of aqueous phase conditions that modulated $^{\bullet}NO_2$ diffusion to the RCM. Under the specific employed conditions of initial 100 μM AH_2, $^{\bullet}NO_2$ delivery rate, aqueous phase mixing (tilting), total aqueous phase surface area, and exposure time, there was a sufficient initial AH_2 pool to enable continued reaction which served to scavenge $^{\bullet}NO_2$, thus constraining diffusion which prevented membrane protein nitration.

Using our well-established flask exposure approach to determine relative reactivities [30], we compared the ability of DFO, HBED, SHA, HU, and AH_2 to drive $^{\bullet}NO_2$ reactive absorption and estimate $^{\bullet}NO_2$ uptake:NO_2^- formation ratios. As illustrated in Figure 4, compared to AH_2, the hydroxamic acids all showed relatively modest reactivity towards $^{\bullet}NO_2$. Previous studies have shown a 1:1 ratio between $^{\bullet}NO_2$ uptake and NO_2^- formation for a variety of substrates [30,32], which generally held true herein. Deviations from a 1:1 ratio were likely due to $^{\bullet}NO_2$ mass balance measurement errors since DFO-mediated $^{\bullet}NO_2$ uptake rates, for example, were quite low relative to $^{\bullet}NO_2$ delivery but $^{\bullet}NO_2$ inflow rates needed to be sufficient to preclude $^{\bullet}NO_2$ as the limiting reagent. On the other hand, both 50 and 100 μM AH_2 displayed approximately equivalent uptake and NO_2^- formation, likely due to saturation of the interfacial transfer rates, which we have previously documented [37]. Furthermore, 30 min exposures of greater AH_2 volumes (with DTPA to reduce adventitious Fe-initiated autoxidation; volumes permitted multiple sample withdrawals) resulted in appreciable loss of reduced ascorbate while only marginal oxidation of DFO could be detected (Supplementary Data). Although it is difficult to completely rule out that DFO is a direct $^{\bullet}NO_2$ scavenger in our model system (see Fig 6), one may rank DFO against AH_2 for this capacity on the basis of $^{\bullet}NO_2$ flux calculated from the decrease in substrate (DFO or AH_2) during a 30 min exposure (see Supplementary Data) assuming the same reaction stoichiometry for both substrates (Substrate:$^{\bullet}NO_2$ = 1:2). The substrate decay rates are coupled to $^{\bullet}NO_2$ flux and reflect reactivities for NO_2. The $^{\bullet}NO_2$ flux into DFO was small (57 ± 21 nmoles $^{\bullet}NO_2$/10 min) and can be compared to the large flux into AH_2 (374 ± 28 nmoles/10 min) (Table S1). It is interesting to note that with AH_2, the decay in

concentration is nearly independent of the [AH_2] from 50 down to 20 μM, strongly suggesting interfacial saturating conditions. Thus, the $^{\bullet}NO_2$ flux with AH_2 ~ 7× larger than for DFO but would be even larger if the interface was not under saturation conditions. Moreover, the NO_2^- formation data presented in Figure 4 suggests that some DFO may be decaying by reacting with $(NO_2)_{solute}$ by simple diffusion rather than by driving $^{\bullet}NO_2$ reactive uptake. These analyses indicate that DFO is a considerably less effective direct scavenger of $^{\bullet}NO_2$ than AH_2 and thus a direct scavenging mechanism is less likely to occur with DFO.

We subsequently compared the ability of the tested hydroxamic acids to inhibit $^{\bullet}NO_2$ exposure-mediated RCM nitration. Table 2 displays notable differences across the various moieties. Compared to 50 μM DFO, which inhibited 3-NT formation to below detectable levels, 200 μM SHA (below detection) and 200 μM BHA (largely) also inhibited membrane nitration. At a somewhat lower concentration, to more closely mimic therapeutic situations, 25 μM HU also displayed notable, but not complete, inhibitory activity. However, like the other non-hydroxamic acid DTPA, 200 μM HBED poorly inhibited exposure-mediated nitration. Thus DFO served as the most robust inhibitor of $^{\bullet}NO_2$ mediated tyrosine nitration

To determine whether DFO-related 3-NT inhibition occurred preferentially with membrane associated tyrosine residues, we performed aqueous bulk phase studies by directly bubbling $^{\bullet}NO_2$ in air through a solution of free tyrosine with and without DFO. Time dependent samples were obtained and 3-NT formation evaluated via spectrophotometry. Figure 5 shows a representative scan that illustrates 3-NT formation in the absence of DFO. However, with DFO addition we noted substantial nitration inhibition even though tyrosine was in appreciable excess. Exposures were conducted for 120 min which was the time required to generate a readily detectable 3-NT peak via this approach. The lack of complete inhibition by DFO may have been due to its direct but relatively limited reaction with $^{\bullet}NO_2$ and/or the stochastic probability of tyrosyl radicals interacting with continuously supplied $^{\bullet}NO_2$ rather than DFO interception. Under these conditions, per published spectra [42], we did not observe dityrosine accumulation again likely due to the limited probability of two tyrosyl radicals directly interacting. However, the data do illustrate that the DFO inhibitory effect occurred under purely aqueous conditions and thus membrane tyrosine residues that protrude outside the hydrophobic domain may also be affected by its presence.

We subsequently investigated the consequences of DFO-Fe binding with regard to nitration inhibition. Addition of $FeCl_3$ alone did not alter $^{\bullet}NO_2$ exposure-related RCM nitration (data not shown), suggesting that under these experimental conditions nitration was Fe-independent. Furthermore, preloading DFO with a Fe molar excess ablated inhibition (data not shown), substantiating that the free hydroxamic moieties were likely responsible for preventing $^{\bullet}NO_2$-mediated nitration. To further test these assumptions regarding Fe-independence and hydroxamic acid-dependence, we preincubated adhered, lysed RCM with either DFO or DTPA and conducted $^{\bullet}NO_2$ exposures with either PO_4 buffer alone or the other chelator present (Table 3). DTPA removal of adventitious iron followed by $^{\bullet}NO_2$ + PO_4 exposures resulted in extensive 3-NT formation. However, DTPA pretreatment followed by exposures containing DFO limited nitration below detection. Conversely, pretreatment with DFO followed by exposures with either PO_4 alone or DTPA resulted in no discernible diminution of 3-NT formation, suggesting that inhibition required the presence of DFO during $^{\bullet}NO_2$ exposure regardless of any pretreatments.

Lastly, in an attempt to mimic what might transpire on the lung surface wherein activated neutrophils in close approximation to epithelial apical membranes could drive cellular nitration reactions via peroxidase activity, MPO was “bound” to RCM prior to addition of NO_2^-/H_2O_2 and DFO (Table 4). Adhered RCM incubation with MPO, followed by

thorough washing, resulted in appreciable remaining MPO activity within the Petri dishes. In combination, MPO + NO_2^- + H_2O_2 generated extensive RCM nitration, as anticipated [19,45]. In the absence of either NO_2^- or H_2O_2 no detectable nitration occurred and, under these experimental conditions, NO_2^- + H_2O_2 in the absence of MPO also did not generate 3-NT. Addition of the MPO inhibitor 4-aminobenzoic hydrazide to MPO + NO_2^- + H_2O_2 also completely blocked 3-NT formation, confirming the requirement for MPO catalytic activity. Importantly, addition of 50 μM DFO to the aqueous phase also limited nitration to below detection even though the RCM-bound MPO should have been generating its nitrating species in very close proximity to the RCM surfaces. Because at these low DFO concentrations MPO catalytic activity was essentially unaffected (data not shown), the results suggest that DFO had sufficient diffusivity within and/or along the RCM to block nitration. Thus, partitioning of DFO into the membranes likely contributed to its inhibitory actions rather than exclusive interception of $(^{\bullet}NO_2)_{solute}$ diffusing from the gas-liquid interface and/or $^{\bullet}NO_2$ generated at the RCM surfaces via MPO activity.

Discussion

$^{\bullet}NO_2$ is now recognized as a ubiquitous oxidant that is derived from both exogenous and endogenous sources. The lung surface is relatively unique because of the composite exposure potentials stemming from direct $^{\bullet}NO_2$ inhalation and/or intrapulmonary oxidation of inhaled $^{\bullet}NO$, and responses to numerous stimuli, including inflammation, which endogenously generate $^{\bullet}NO_2$. Because $^{\bullet}NO_2$ is central in the overall biology of reactive nitrogen species (RNS) [11–13] and because protein tyrosine nitration, wherein $^{\bullet}NO_2$ serves as the terminal nitrating species, is widely considered a hallmark index of RNS biochemical interactions, it is important to elucidate the factors that might modulate the net generation of nitrated tyrosine residues.

Due to its high affinity binding, DFO is the most commonly employed Fe chelator and has been used in numerous studies to identify the importance of Fe in redox reactions (*e.g.*, Fenton chemistry) as well as its active site contributions in protein catalysis. Although the binding affinities are somewhat less, other hydroxamic acids chelate metals as well. Previous observations, both direct and inferential [3,4,7–9,34]), have suggested that DFO may function beyond its Fe binding activities. Other related chemical species, such as HU, have broad applicability as therapeutic agents with a variety of proposed pharmacologic modalities, including, for example, inhibition of enzymes such as ribonucleotide reductase (*e.g.,* [46,47]). Since transient radicals, including tyrosyl, are key in the catalytic actions of numerous proteins [48,49] and since tyrosine nitration has been shown to affect function in diverse proteins [50–58], elucidating whether DFO and other hydroxamic acids may modulate nitration reactions and biological functions independent of chelation is important for understanding mechanisms, and how hydroxamic acids may influence and potentially confound *in vitro* and *in vivo* experimental outcomes and interpretations.

To clarify the extent that reagent DFO might confound studies focused on protein nitration reactions and Fe contributions, a minimalist approach was utilized that incorporated both a well-defined nitration target (RCM) and gas phase $^{\bullet}NO_2$ exposures. Although the RCM model system involves mass transfer and reaction/diffusion complexities, delivery of gas phase $^{\bullet}NO_2$ (stable $^{\bullet}NO_2$ aqueous solutions cannot be generated/employed) limits it to the sole RNS introduced and avoids potential confounding from other reactive species generated by use of $^{\bullet}NO_2$ precursors (*e.g.,* $ONOOCO_2^-$), flash photolysis, or pulse radiolysis [7,12,32–35,59], thus affording a methodologic advantage.

Figures 2 and 3 illustrate that DFO effectively prevented membrane protein nitration at very low concentrations (≤ 5 μM) and over a relatively prolonged exposure period (≥ 90 min).

Considering that $^{\bullet}NO_2$ was not the limiting reagent, due to the steady state exposure conditions, and that DFO was a relatively poor substrate for $^{\bullet}NO_2$ reactive absorption (Fig. 4 and Fig. S1), it does not seem likely that 3-NT inhibition resulted solely from direct $(^{\bullet}NO_2)_{solute}$ scavenging. In this regard, a rate constant for reaction of DFO with $^{\bullet}NO_2$ has been reported ($k = 7.6 \times 10^6\ M^{-1}s^{-1}$ [7]) which is smaller than the rate constant for AH_2 with $^{\bullet}NO_2$ (two values in general agreement with one another have been reported for ascorbate; $1.8 \times 10^7\ M^{-1}s^{-1}$ and $3.5 \times 10^7\ M^{-1}s^{-1}$ [53,60,61]). It is interesting to note that to the best of our knowledge, the rate constant reported for DFO with $^{\bullet}NO_2$ is the only rate constant regarding a complex hydroxamic acid. Recently, Samuni and Goldstein reported that the rate constant for acetohydroxamic acid, the simplest member of the hydroxamic acid series, is less than $2 \times 10^4\ M^{-1}s^{-1}$ [62] which contrasts sharply with the larger value reported for DFO [7] and argues against direct scavenging of $^{\bullet}NO_2$ by DFO.

Ascorbate, which is a more facile $^{\bullet}NO_2$ reactant than DFO, showed some degree of 3-NT inhibition at initial concentrations as low as 25 μM. It should be noted that AH_2 will be consumed during the course of exposure so that $^{\bullet}NO_2$ diffusion through the overlying aqueous film is a balance among its delivery and interfacial mass transfer rates, diffusion of both solute $^{\bullet}NO_2$ and aqueous substrate, rate of aqueous substrate consumption, and depth of the aqueous film, among others. Thus, if the facile reactive substrate concentrations drop below a critical threshold, $^{\bullet}NO_2$ diffusion to directly interact with the RCM becomes more favorable. Consequently, Table 1 shows that in the presence of a sufficiently large initial substrate pool, $^{\bullet}NO_2$ was consumed via reaction and although secondary oxidants may have been produced thereby driving RCM oxidation, insufficient $^{\bullet}NO_2$ reached the membranes to add to any existing tyrosyl radicals. If aqueous antioxidant concentrations remain sufficiently elevated, both $^{\bullet}NO_2$ and secondary oxidants may be quenched thereby preventing or repairing tyrosine oxidation and thus limit consequent nitration.

The DFO-Fe complex can function as a reductant when in the DFO-Fe^{2+} state [63]. Because our use of lysed red blood cells, and results from previous studies, document the presence of adventitious iron, such a potential mechanism for tyrosyl radical reduction should not be ignored. However, although the DFO bound Fe may remain redox active, it would require a constant source of electrons during $^{\bullet}NO_2$ exposure to maintain its reductive capacity. We believe that the presence of appreciable DFO-Fe^{2+} in our system was unlikely since an applicable electron source was present only during the AH_2 studies. Even then, the continuous $^{\bullet}NO_2$ influx would have likely resulted in preferential $^{\bullet}NO_2$ reduction over tyrosyl radical repair. In the absence of aqueous phase AH_2, no obvious electron source would have been available. Despite the complexities of Fe redox activities, our studies utilizing ferrioxamine or adventitious Fe removal tend to confirm this. Iron-saturated DFO had no inhibitory capacity and adventitious Fe removal (Table 3) required DFO *per se* present to block $^{\bullet}NO_2$-mediated membrane nitration.

The ability of DFO to inhibit nitration occurred under a variety of physicochemical situations in both aqueous and hydrophobic compartments. Figure 5 illustrates that DFO constrained nitration under purely aqueous phase conditions while Table 4 demonstrates similar results with oxidants and/or nitrating species generated via MPO activity at or near membrane surfaces. We also considered DFO may directly inhibit MPO since it has been reported that certain hydroxamic acids may compete with MPO substrates (chloride, thiocyanate, and nitrite) for binding to the same active site, although inhibition was only observed at higher hydroxamic acid concentrations than we employed [64,65]. Interestingly, a published report on the inhibition of MPO by SHA used guaiacol (a phenolic compound) as a co-substrate for MPO [64]. We believe these results could have been confused by reaction of SHA with the guaiacol phenoxyl radicals because we did not observe MPO inhibition by DFO at the highest concentration levels we employed while using 3,3′,5,5′-

tetramethylbenzidine as a co-substrate for MPO (data not shown). Thus, based on our empirical observations of sustained MPO catalytic activity in the presence of 50 μM DFO, we dismissed competitive inhibition of MPO as a mechanism for 3-NT inhibition during the MPO/DFO studies.

Irrespective of the $^{\bullet}NO_2$ source (gas phase; MPO), it is difficult to precisely discern where within the membrane structure nitration occurred but, despite the lack of a "lens" effect driving preferential $^{\bullet}NO_2$ partitioning into the membrane hydrophobic regions [21], one would anticipate nitration of tyrosines both within and protruding out of the membrane proper. The aqueous bulk phase studies showed a right spectral shift in the DFO+Tyr scans (Fig. 5; 325–375 nm) which may be attributable to oxidation products including adducts such as DFO-NO_2, DFO-Tyr, etc., among a variety of others. Further analyses are needed to resolve the precise genesis of the spectral shift. However, this does not detract from the observations that even under bulk phase, well mixed conditions, the presence of DFO appreciably reduced the extent of 3-NT formation. Although dityrosine formation has been observed in a number of studies [59,62,66], its apparent absence herein was reasonable given the tyrosyl radical generation constraints under these study conditions.

Regardless of the mechanism(s) by which tyrosine oxidation occurred, we propose that DFO predominantly inhibited its nitration according to the mechanism below where R$^{\bullet}$ represents a free radical such as $^{\bullet}NO_2$ or a lipid-derived radical:

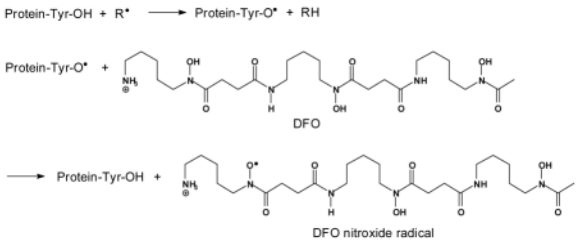

The site of radical formation in DFO is in accordance to the structure proposed by Morehouse *et. al.* [67]. Per the above, DFO competes with $^{\bullet}NO_2$ for reaction with protein tyrosyl radicals, repairs the oxidized tyrosine residues, and inhibits nitration. DFO is only slightly lipophilic and based on its octanol-water partition coefficient, approximately 1.4% of the aqueous concentration should have partitioned into the lipid bilayer [68]. However, we believe that both aqueous and membrane-associated DFO participated in membrane protein tyrosyl radical reduction with the former reducing the exposed tyrosyl radicals while the latter reduced tyrosyl radicals embedded deeper in the membrane.

For our experimental conditions, DFO was likely to be present (both in membranes and the aqueous milieu) at higher concentration than $^{\bullet}NO_2$ since $^{\bullet}NO_2$ is sparingly soluble in aqueous media [69] and only slightly more soluble in organic media [70,71]. Moreover, recent analyses suggest that $^{\bullet}NO_2$ does not partition into membranes to the same extent and thus undergo accelerated reaction as has been shown for $^{\bullet}NO$ [20,21]. The rate constants for the tyrosyl radical and DFO reactions with $^{\bullet}NO_2$ are 3×10^9 $M^{-1}s^{-1}$ and 6.3×10^6, respectively [72]; protein tyrosyl radicals are probably somewhat less reactive than tyrosyl radicals. Although the rate constant for nitration is some 400 times larger than the published rate constant for reaction with DFO, because [DFO] is expected to be much larger than [$^{\bullet}NO_2$] at the reaction sites, we expect DFO to outcompete $^{\bullet}NO_2$ for the protein tyrosyl radicals. In this regard, one can calculate using a Henry's law constant equal to 1.4×10^{-2} M atm^{-1} [70] and ideal gas behavior that for a gas phase [$^{\bullet}NO_2$] equal to 4.5 ppm, the [$^{\bullet}NO_2$] in the aqueous phase will approximate 4.5×10^{-6} atm $\times$ 1.4×10^{-2} M atm = 6.3×10^{-8} M. This value should be

$$\frac{\text{rate of repair}}{\text{rate of nitration}} = \frac{k_{TyrO\bullet/DFO}[TyrO\bullet][DFO]}{k_{TyrO\bullet/NO_2}[TyrO\bullet][NO_2]} = \frac{k_{TyrO\bullet/DFO}[DFO]}{k_{TyrO\bullet/NO_2}[NO_2]} \geq \frac{(6.3\times10^{6}\mathrm{M}^{-1}\mathrm{s}^{-1})(50\times10^{-6}\mathrm{M})}{(3\times10^{9}\mathrm{M}^{-1}\mathrm{s}^{-1})(6.3\times10^{-8}\mathrm{M})} \approx 2$$

taken as an upper limit because of the high reactivity of $^{\bullet}NO_2$ but can be compared to the aqueous [DFO] equal to 50 μM used in our experiments, which is some 800 times larger than the calculated equilibrium [$^{\bullet}NO_2$]. Consequently, it is reasonable to assume that in the aqueous compartment, the relatively greater DFO concentration could more than compensate for its lower reactivity with tyrosyl radicals, compared to $^{\bullet}NO_2$. Thus in compilation, a conservative comparison of the rate of DFO repair versus the rate of $^{\bullet}NO_2$ addition suggests that repair is favored in excess of two-fold over nitration. Any decrease in the rate constant that describes the DFO + $^{\bullet}NO_2$ reaction would increase the computed repair preferentiality.

We found that tyrosine nitration was completely inhibited by DFO, suggesting effective competition of DFO for trans-membrane protein tyrosyl radicals as well. This may be due to a steep [$^{\bullet}NO_2$] gradient with the membrane concentration being much lower than what occurs in aqueous solution. This would be a kinetic rather than a thermodynamic effect because $^{\bullet}NO_2$ is slightly lipophilic [21,70,71] and may be due to faster consumption of $^{\bullet}NO_2$ (by chemical reactions in the membrane) than diffusion of $^{\bullet}NO_2$ into the membrane. Figure 6 is a schematic cartoon depicting these numerous complexities and contributory factors.

In further support for our mechanism, hydroxamic acids and hydroxyl-amines have been reported to reduce the active site tyrosyl radical of ribonucleotide reductase, which is consistent with reports of DFO and HU inhibiting this enzyme [46,47]. Consequently, application of hydroxamic acids could affect the catalytic activities of other proteins with active site tyrosyl radicals. Non-enzymatic proteins may be important considerations as well [52,54,56–58] since tyrosine nitration of signaling molecules may also disrupt their normal function. Tyrosine nitration may affect protein function and structure, and change the rate of proteolytic degradation of nitrated proteins. Nitration often leads to loss of protein activity but recent proteomic analyses have revealed that a variety of cellular processes may be affected by protein tyrosine nitration in various ways. These processes include energy metabolism, protein, nucleic acid and ion binding, cellular structure and regulation, enzymatic activity control, and cellular signaling, including apoptosis. Thus, therapeutic intervention with hydroxamic acids when their intended use is to chelate ferric ions or inhibit histone deacetylases may have secondary effects. Further investigations are needed to determine whether these secondary effects due to inhibition of protein tyrosine nitration could be beneficiary, or detrimental, against a background of poisoning or disease wherein protein tyrosine nitration levels are found to be elevated.

Numerous investigations have utilized DFO to identify Fe as a critical effecter driving redox perturbations. However, although DFO will clearly sequester Fe, and has been shown to inhibit peroxynitrite-related interactions, if DFO is used as an investigational reagent the precise mechanisms by which altered outcomes occur may not simply involve removal of redox active Fe, limiting nutraceutical Fe availability, or scavenging of oxidant and/or nitrating species but rather, direct action on tyrosyl radical intermediates. Furthermore, DFO enters the cell mostly via endocytosis, which is the same pathway as transferrin, and thus during lysosomal maturation and acidification the Fe is liberated to form “free” redox active (Fenton) Fe. Thus, DFO may serve as an “antioxidant”, Fe chelator, and radical scavenger. Indeed a major new clinical form of DFO is “starch-DFO” which apparently confines its entry to endocytic pathways [73,74]. Such factors need to be considered, for example, if DFO is added to tissue culture media to help preserve supplemental AH_2, is included in lung

lavage fluids to reduce artifactual antioxidant oxidation, or if administered *in vivo* if subsequent cell biology studies are to be performed. Consequently, because of the varied functions of DFO, there may be a need to reevaluate some proposed mechanisms related to Fe-mediated events/interactions via the use of non-hydroxamic acid chelators (*e.g.* DTPA) and a requisite need to both interpret experimental results with appropriate caution and include confirmatory studies using ancillary approaches.

Supplementary Material

Refer to Web version on PubMed Central for supplementary material.

Acknowledgments

This work was supported in part by NIH grants R01 HL 54696 (EMP) and P01 ES11617 (EMP). Exposure capabilities were made available through the UAB Environmental Exposure Facility.

Reference List

1. Martell, AE.; Smith, RM. Critical Stability Constants. New York: Plenum Press; 1974.
2. Link G, Pinson A, Hershko C. Ability of the orally effective iron chelators dimethyl- and diethyl-hydroxypyrid-4-one and of deferoxamine to restore sarcolemmal thiolic enzyme activity in iron-loaded heart cells. Blood. 1994; 83:2692–2697. [PubMed: 8167347]
3. Davies MJ, Donkor R, Dunster CA, Gee CA, Jonas S, Willson RL. Desferrioxamine (Desferal) and superoxide free radicals. Formation of an enzyme-damaging nitroxide. Biochem J. 1987; 246:725–729. [PubMed: 2825650]
4. Halliwell B. Protection against tissue damage in vivo by desferrioxamine: what is its mechanism of action? Free Radic Biol Med. 1989; 7:645–651. [PubMed: 2695408]
5. LaLonde C, Ikegami K, Demling R. Aerosolized deferoxamine prevents lung and systemic injury caused by smoke inhalation. J Appl Physiol. 1994; 77:2057–2064. [PubMed: 7532647]
6. Meulenbelt J, Dormans JA, van BL, Rombout PJ, Sangster B. Desferrioxamine treatment reduces histological evidence of lung damage in rats after acute nitrogen dioxide (NO2) intoxication. Hum Exp Toxicol. 1993; 12:389–395. [PubMed: 7902116]
7. Bartesaghi S, Trujillo M, Denicola A, Folkes L, Wardman P, Radi R. Reactions of desferrioxamine with peroxynitrite-derived carbonate and nitrogen dioxide radicals. Free Radic Biol Med. 2004; 36:471–483. [PubMed: 14975450]
8. Denicola A, Souza JM, Gatti RM, Augusto O, Radi R. Desferrioxamine inhibition of the hydroxyl radical-like reactivity of peroxynitrite: role of the hydroxamic groups. Free Radic Biol Med. 1995; 19:11–19. [PubMed: 7635352]
9. Kanner J, Harel S. Desferrioxamine as an electron donor. Inhibition of membranal lipid peroxidation initiated by H2O2-activated metmyoglobin and other peroxidizing systems. Free Radic Res Commun. 1987; 3:309–317. [PubMed: 3149948]
10. Bartesaghi S, Valez V, Trujillo M, Peluffo G, Romero N, Zhang H, Kalyanaraman B, Radi R. Mechanistic studies of peroxynitrite-mediated tyrosine nitration in membranes using the hydrophobic probe N-t-BOC-L-tyrosine tert-butyl ester. Biochemistry. 2006; 45:6813–6825. [PubMed: 16734418]
11. Hill BG, Dranka BP, Bailey SM, Lancaster JR, rley-Usmar VM. What Part of NO Don't You Understand? Some Answers to the Cardinal Questions in Nitric Oxide Biology. Journal of Biological Chemistry. 2010; 285:19699–19704. [PubMed: 20410298]
12. Pryor WA, Houk KN, Foote CS, Fukuto JM, Ignarro LJ, Squadrito GL, Davies KJA. Free radical biology and medicine: it's a gas, man! American Journal of Physiology-Regulatory Integrative and Comparative Physiology. 2006; 291:R491–R511.
13. Souza JM, Peluffo G, Radi R. Protein tyrosine nitration - Functional alteration or just a biomarker? Free Radical Biology and Medicine. 2008; 45:357–366. [PubMed: 18460345]

14. Baldus S, Castro L, Eiserich JP, Freeman BA. Is NO news bad news in acute respiratory distress syndrome? American Journal of Respiratory and Critical Care Medicine. 2001; 163:308–310. [PubMed: 11179096]
15. Baldus S, Eiserich JP, Brennan ML, Jackson RM, Alexander CB, Freeman BA. Spatial mapping of pulmonary and vascular nitrotyrosine reveals the pivotal role of myeloperoxidase as a catalyst for tyrosine nitration in inflammatory diseases. Free Radical Biology and Medicine. 2002; 33:1010–1019. [PubMed: 12361810]
16. Davis IC, Zajac AJ, Nolte KB, Botten J, Hjelle B, Matalon S. Elevated generation of reactive oxygen/nitrogen species in hantavirus cardiopulmonary syndrome. J Virol. 2002; 76:8347–8359. [PubMed: 12134039]
17. Sittipunt C, Steinberg KP, Ruzinski JT, Myles C, Zhu S, Goodman RB, Hudson LD, Matalon S, Martin TR. Nitric oxide and nitrotyrosine in the lungs of patients with acute respiratory distress syndrome. American Journal of Respiratory and Critical Care Medicine. 2001; 163:503–510. [PubMed: 11179131]
18. Integrated Science Assessment for Oxides of Nitrogen -- Health Criteria. U.S. Environmental Protection Agency; 2008.
19. Eiserich JP, Hristova M, Cross CE, Jones AD, Freeman BA, Halliwell B, van der Vliet A. Formation of nitric oxide derived inflammatory oxidants by myeloperoxidase in neutrophils. Nature. 1998; 391:393–397. [PubMed: 9450756]
20. Liu XP, Miller MJS, Joshi MS, Thomas DD, Lancaster JR. Accelerated reaction of nitric oxide with O-2 within the hydrophobic interior of biological membranes. Proceedings of the National Academy of Sciences of the United States of America. 1998; 95:2175–2179. [PubMed: 9482858]
21. Squadrito GL, Postlethwait EM. On the hydrophobicity of nitrogen dioxide: Could there be a “lens” effect for NO2 reaction kinetics? Nitric Oxide-Biology and Chemistry. 2009; 21:104–109.
22. Bidani, A.; Postlethwait, EM. Complexities in Structure and Function of the Lung (Lung Biology in Health and Disease). New York: Marcell Dekker, Inc; 1998. Kinetic Determinants of Reactive Gas Uptake; p. 243-295.
23. Postlethwait EM, Bidani A. Mechanisms of Pulmonary NO2 Absorption. Toxicology. 1994; 89:217–237. [PubMed: 8023330]
24. Hesterberg TW, Bunn WB, McClellan RO, Hamade AK, Long CM, Valberg PA. Critical review of the human data on short-term nitrogen dioxide (NO(2)) exposures: Evidence for NO(2) no-effect levels. Critical Reviews in Toxicology. 2009; 39:743–781. [PubMed: 19852560]
25. Kirsch M, Korth HG, Sustmann R, de Groot H. The pathobiochemistry of nitrogen dioxide. Biological Chemistry. 2002; 383:389–399. [PubMed: 12033430]
26. Latza U, Gerdes S, Baur X. Effects of nitrogen dioxide on human health: Systematic review of experimental and epidemiological studies conducted between 2002 and 2006. International Journal of Hygiene and Environmental Health. 2009; 212:271–287. [PubMed: 18771952]
27. Postlethwait EM, Bidani A. Reactive Uptake Governs the Pulmonary Air Space Removal of Inhaled Nitrogen-Dioxide. Journal of Applied Physiology. 1990; 68:594–603. [PubMed: 2318771]
28. Postlethwait EM, Langford SD, Bidani A. Kinetics of NO2 Air Space Absorption in Isolated Rat Lungs. Journal of Applied Physiology. 1992; 73:1939–1945. [PubMed: 1474071]
29. Ford E, Hughes MN, Wardman P. Kinetics of the reactions of nitrogen dioxide with glutathione, cysteine, and uric acid at physiological pH. Free Radic Biol Med. 2002; 32:1314–1323. [PubMed: 12057769]
30. Postlethwait EM, Langford SD, Jacobson LM, Bidani A. NO2 Reactive Absorption Substrates in Rat Pulmonary Surface Lining Fluids. Free Radical Biology and Medicine. 1995; 19:553–563. [PubMed: 8529914]
31. Bastacky J, Lee CY, Goerke J, Koushafar H, Yager D, Kenaga L, Speed TP, Chen Y, Clements JA. Alveolar lining layer is thin and continuous: low-temperature scanning electron microscopy of rat lung. J Appl Physiol. 1995; 79:1615–1628. [PubMed: 8594022]
32. Velsor LW, Ballinger CA, Patel J, Postlethwait EM. Influence of epithelial lining fluid lipids on NO(2)-induced membrane oxidation and nitration. Free Radic Biol Med. 2003; 34:720–733. [PubMed: 12633749]

33. Velsor LW, Postlethwait EM. NO2-induced generation of extracellular reactive oxygen is mediated by epithelial lining layer antioxidants. Am J Physiol. 1997; 273:L1265–L1275. [PubMed: 9435583]
34. Bartesaghi S, Wenzel J, Trujillo M, Lopez M, Joseph J, Kalyanaraman B, Radi R. Lipid peroxyl radicals mediate tyrosine dimerization and nitration in membranes 2. Chem Res Toxicol. 2010; 23:821–835. [PubMed: 20170094]
35. Avner, Treinin; Elie, Hayon. Absorption spectra and reaction kinetics of NO2, N2O3, and N2O4 in aqueous solution. J Amer Chem Soc. 1970; 92(20):5821–5828. Ref Type: Journal (Full).
36. Nielson DW, Goerke J, Clements JA. Alveolar subphase pH in the lungs of anesthetized rabbits. Proc Natl Acad Sci U S A. 1981; 78:7119–7123. [PubMed: 6947276]
37. Postlethwait EM, Langford SD, Bidani A. Interfacial transfer kinetics of NO2 into pulmonary epithelial lining fluid. J Appl Physiol. 1991; 71:1502–1510. [PubMed: 1757376]
38. Suzuki K, Ota H, Sasagawa S, Sakatani T, Fujikura T. Assay method for myeloperoxidase in human polymorphonuclear leukocytes. Anal Biochem. 1983; 132:345–352. [PubMed: 6312841]
39. Giustarini D, Rossi R, Milzani A, le-Donne I. Nitrite and nitrate measurement by Griess reagent in human plasma: evaluation of interferences and standardization. Methods Enzymol. 2008; 440:361–380. [PubMed: 18423230]
40. Buettner GR. In the absence of catalytic metals ascorbate does not autoxidize at pH 7: ascorbate as a test for catalytic metals. J Biochem Biophys Methods. 1988; 16:27–40. [PubMed: 3135299]
41. Monzyk B, Crumbliss AL. Kinetics and mechanism of the stepwise dissociation of iron(III) from ferrioxamine B in aqueous acid. J Am Chem Soc. 1982; 104:4921–4929.
42. Malencik DA, Sprouse JF, Swanson CA, Anderson SR. Dityrosine: preparation, isolation, and analysis. Anal Biochem. 1996; 242:202–213. [PubMed: 8937563]
43. Mallozzi C, Di Stasi AM, Minetti M. Peroxynitrite modulates tyrosine-dependent signal transduction pathway of human erythrocyte band 3. FASEB J. 1997; 11:1281–1290. [PubMed: 9409547]
44. Grzelak A, Balcerczyk A, Mateja A, Bartosz G. Hemoglobin can nitrate itself and other proteins. Biochim Biophys Acta. 2001; 1528:97–100. [PubMed: 11687295]
45. Burner U, Furtmuller PG, Kettle AJ, Koppenol WH, Obinger C. Mechanism of reaction of myeloperoxidase with nitrite. J Biol Chem. 2000; 275:20597–20601. [PubMed: 10777476]
46. Saban N, Bujak M. Hydroxyurea and hydroxamic acid derivatives as antitumor drugs. Cancer Chemother Pharmacol. 2009; 64:213–221. [PubMed: 19350240]
47. Shao J, Zhou B, Zhu L, Bilio AJ, Su L, Yuan YC, Ren S, Lien EJ, Shih J, Yen Y. Determination of the potency and subunit-selectivity of ribonucleotide reductase inhibitors with a recombinant-holoenzyme-based in vitro assay. Biochem Pharmacol. 2005; 69:627–634. [PubMed: 15670581]
48. Fontecave M, Pierre JL. Mechanisms of formation of free radicals in biological catalysis. Comptes Rendus de l Academie des Sciences Serie Ii Fascicule C-Chimie. 2001; 4:531–538.
49. Stubbe JA, van der Donk WA. Protein radicals in enzyme catalysis (vol 98, pg 705, 1998). Chemical Reviews. 1998; 98:2661. [PubMed: 11848974]
50. Aguiar M, Masse R, Gibbs BF. Regulation of cytochrome P450 by posttranslational modification. Drug Metabolism Reviews. 2005; 37:379–404. [PubMed: 15931769]
51. Eiserich JP, Estevez AG, Bamberg TV, Ye YZ, Chumley PH, Beckman JS, Freeman BA. Microtubule dysfunction by posttranslational nitrotyrosination of alpha-tubulin: A nitric oxide-dependent mechanism of cellular injury. Proceedings of the National Academy of Sciences of the United States of America. 1999; 96:6365–6370. [PubMed: 10339593]
52. Greenacre SAB, Ischiropoulos H. Tyrosine nitration: Localisation, quantification, consequences for protein function and signal transduction. Free Radical Research. 2001; 34:541–581. [PubMed: 11697033]
53. Jang B, Han S. Biochemical properties of cytochrome c nitrated by peroxynitrite. Biochimie. 2006; 88:53–58. [PubMed: 16040185]
54. Matalon S, Shrestha K, Kirk M, Waldheuser S, McDonald B, Smith K, Gao ZQ, Belaaouaj A, Crouch EC. Modification of surfactant protein D by reactive oxygen-nitrogen intermediates is accompanied by loss of aggregating activity, in vitro and in vivo. Faseb Journal. 2009; 23:1415–1430. [PubMed: 19126597]

55. Millan-Crow LA, Cruthirds DL. Invited review - Manganese superoxide dismutase in disease. Free Radical Research. 2001; 34:325–336. [PubMed: 11328670]
56. Park SW, Huq M, Hu XL, Wei LN. Tyrosine nitration on p65 - A novel mechanism to rapidly inactivate nuclear factor-kappa B. Molecular & Cellular Proteomics. 2005; 4:300–309. [PubMed: 15657065]
57. Schopfer FJ, Baker PRS, Freeman BA. NO-dependent protein nitration: a cell signaling event or an oxidative inflammatory response? Trends in Biochemical Sciences. 2003; 28:646–654. [PubMed: 14659696]
58. Siles E, Martinez-Lara E, Nunez MI, Munoz-Gamez JA, Martin-Oliva D, Valenzuela MT, Peinado MA, de Almodovar JMR, Oliver FJ. PARP-1-dependent 3-nitrotyrosine protein modification after DNA damage. Journal of Cellular Biochemistry. 2005; 96:709–715. [PubMed: 16052507]
59. Bartesaghi S, Wenzel J, Trujillo M, Lopez M, Joseph J, Kalyanaraman B, Radi R. Lipid Peroxyl Radicals Mediate Tyrosine Dimerization and Nitration in Membranes. Chemical Research in Toxicology. 2010; 23:821–835. [PubMed: 20170094]
60. Alfassi ZB, Huie RE, Neta P, Shoute LCT. Temperature-Dependence of the Rate Constants for Reaction of Inorganic Radicals with Organic Reductants. Journal of Physical Chemistry. 1990; 94:8800–8805.
61. Forni LG, Mora-Arellano VO, Packer JE, Willson RL. Nitrogen dioxide and related free radicals: electron-transfer reactions with organic compounds in solutions containing nitrite or nitrate. J Chem Soc, Perkin Trans. 1986; 2:1–6.
62. Goldstein S, Czapski G, Lind J, Merenyi G. Tyrosine nitration by simultaneous generation of (.)NO and O-(2) under physiological conditions. How the radicals do the job. J Biol Chem. 2000; 275:3031–3036. [PubMed: 10652282]
63. Burkitt MJ, Kadiiska MB, Hanna PM, Jordan SJ, Mason RP. Electron-Spin-Resonance Spin-Trapping Investigation Into the Effects of Paraquat and Desferrioxamine on Hydroxyl Radical Generation During Acute Iron Poisoning. Molecular Pharmacology. 1993; 43:257–263. [PubMed: 8381512]
64. Ikeda-Saito M, Shelley DA, Lu L, Booth KS, Caughey WS, Kimura S. Salicylhydroxamic acid inhibits myeloperoxidase activity. J Biol Chem. 1991; 266:3611–3616. [PubMed: 1847381]
65. Klebanoff SJ, Waltersdorph AM. Inhibition of peroxidase-catalyzed reactions by deferoxamine. Arch Biochem Biophys. 1988; 264:600–606. [PubMed: 2840860]
66. Lim CH, Dedon PC, Deen WM. Kinetic analysis of intracellular concentrations of reactive nitrogen species. Chem Res Toxicol. 2008; 21:2134–2147. [PubMed: 18828639]
67. Morehouse KM, Flitter WD, Mason RP. The enzymatic oxidation of Desferal to a nitroxide free radical. FEBS Lett. 1987; 222:246–250. [PubMed: 2820803]
68. Ihnat PM, Vennerstrom JL, Robinson DH. Solution equilibria of deferoxamine amides. J Pharm Sci. 2002; 91:1733–1741. [PubMed: 12115836]
69. Sander, R. Compilation of Henry's Law Constants for Inorganic and Organic Species of Potential Importance in Environmental Chemistry (Version 3). 1999. http://www.henrys-law.org
70. Lur'e BA, Arkhipov IV, Apal'kova VN. The N2O4 = 2NO2 Equilibrium in Solutions. Russian Journal of Physical Chemistry. 1986; 60:1144–1147.
71. Mendiara SN, Perissinotti LJ. Dissociation equilibrium of dinitrogen tetroxide in organic solvents: An electron paramagnetic resonance measurement. Applied Magnetic Resonance. 2003; 25:323–346.
72. Prutz WA, Monig H, Butler J, Land EJ. Reactions of nitrogen dioxide in aqueous model systems: oxidation of tyrosine units in peptides and proteins. Arch Biochem Biophys. 1985; 243:125–134. [PubMed: 4062299]
73. Baird SK, Kurz T, Brunk UT. Metallothionein protects against oxidative stress-induced lysosomal destabilization. Biochemical Journal. 2006; 394:275–283. [PubMed: 16236025]
74. Doulias PT, Christoforidis S, Brunk UT, Galaris D. Endosomal and lysosomal effects of desferrioxamine: Protection of HeLa cells from hydrogen peroxide-induced DNA damage and induction of cell-cycle arrest. Free Radical Biology and Medicine. 2003; 35:719–728. [PubMed: 14583336]

Highlights

- DFO robustly inhibits tyrosine nitration (3-NT) independent of Fe chelation.
- The mechanism likely involves tyrosyl radical repair preventing $^{\bullet}NO_2$ addition.
- More facile reactants scavenge $^{\bullet}NO_2$ but lose 3-NT inhibition due to consumption.
- DFO effectively inhibits 3-NT in both aqueous and hydrophobic compartments.
- DFO multifunctionalities should be considered during its reagent and clinical use.

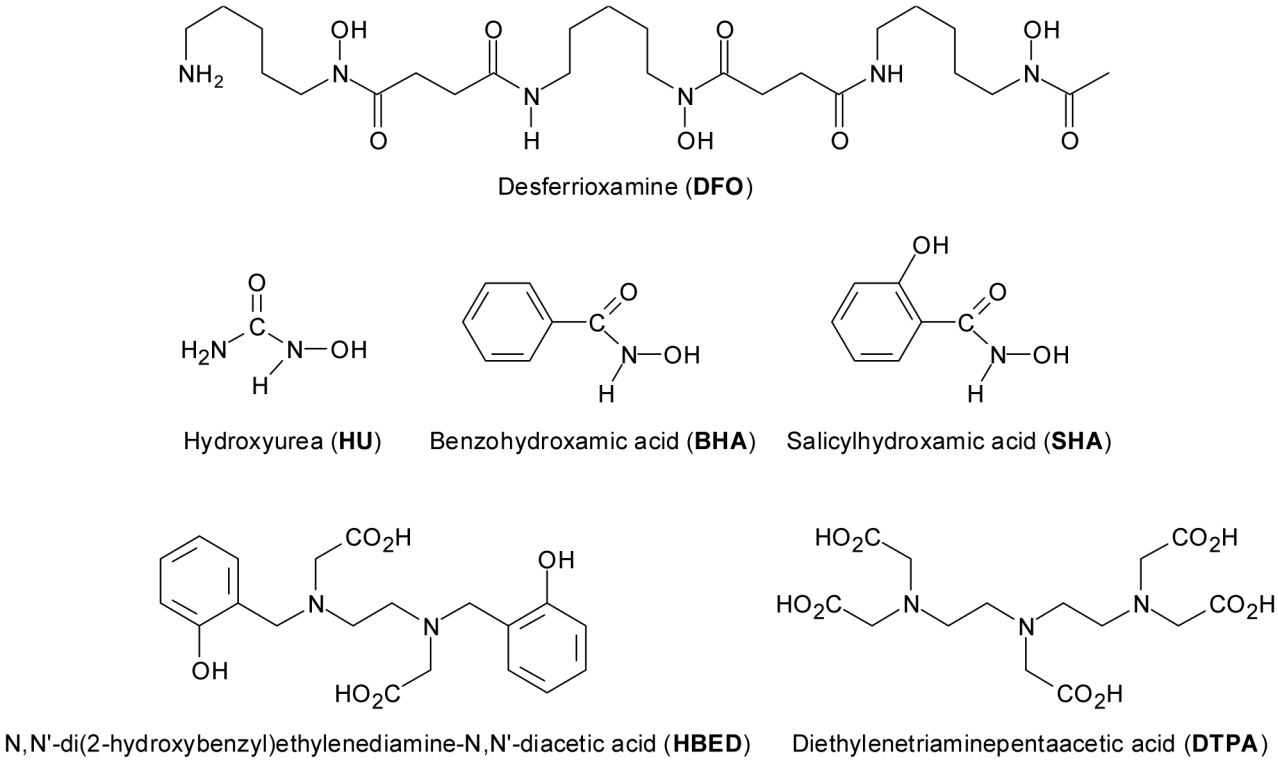

Figure 1. Schematic Structures of Hydroxamic Acids and Related Compounds

Note that DFO contains three hydroxamic groups while HU, BHA, and SHA only a single group. HBED and DTPA are not hydroxamic acids although all five moieties show variable degrees of metal chelation.

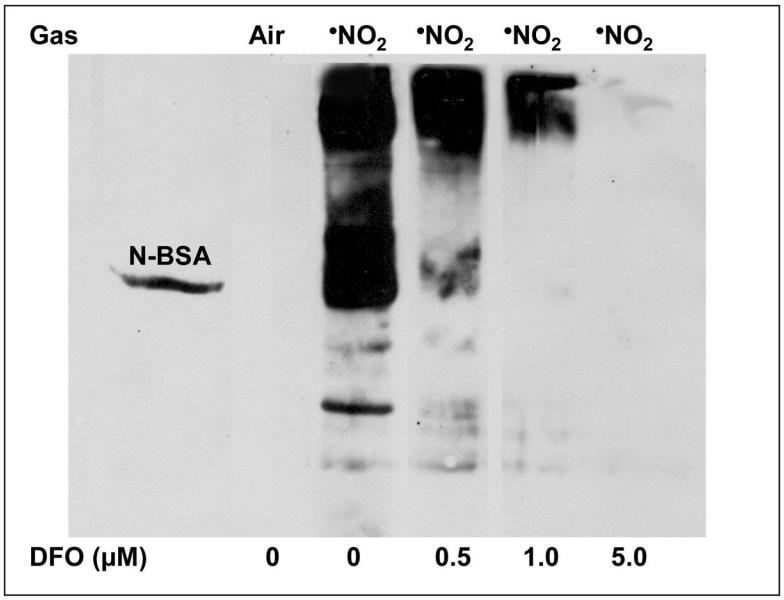

Figure 2. Effect of Initial DFO Concentration on $^{\bullet}NO_2$-Mediated RCM Nitration

RCM, adhered in Petri dishes, were overlain with PO_4 buffer (10 mOms, pH 7.0) plus increasing initial DFO concentrations (0 – 5.0 μM) and exposed to 4.5 ppm $^{\bullet}NO_2$ for 30 min with intermittent cyclic tilting of the glass exposure chamber. DFO was added just prior to exposure onset. Post exposure, RCM were harvested and 3-NT formation assessed via Western analysis as described in Methods ($n \geq 4$ independent RCM preparations and related exposures). Nitrated BSA was utilized as a positive control standard for 3-NT. Illustrated in this exampled gel is the fact that even 5 μM DFO extensively inhibited 3-NT formation (herein scored as "—") while 1 μM constrained formation to little (+) and even 0.5 μM reduced generation to a significant (+++) extent. 0 μM DFO comparatively illustrates our subjective scale of extensive (++++). In the absence of $^{\bullet}NO_2$ exposure, note that basal levels of 3-NT within the adhered RCM were below detectable levels. Differences across the [DFO] were statistically significant.

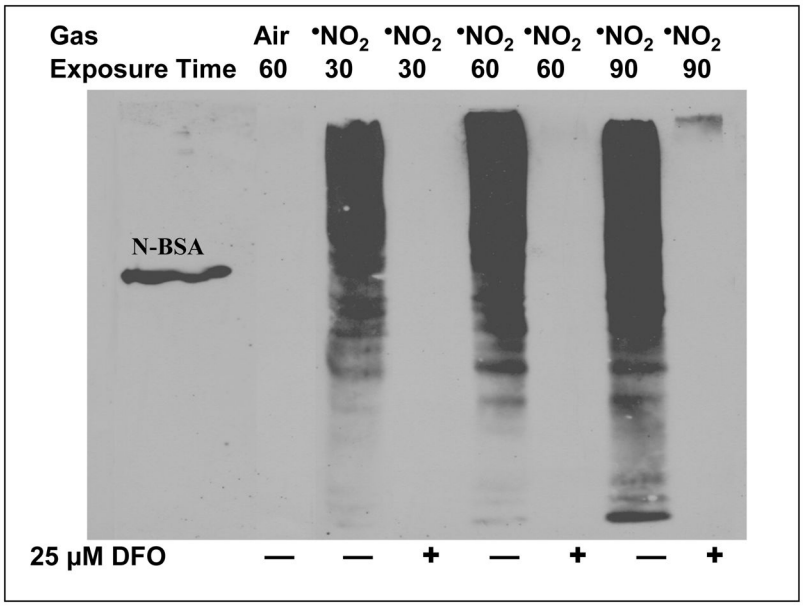

Figure 3. Time Course of $^{\bullet}NO_2$-Mediated RCM Nitration in the Presence and Absence of Desferrioxamine

RCM, adhered in Petri dishes, were overlain with PO_4 buffer (10 mOms, pH 7.0) with and without 25 μM DFO and exposed to 4.5 ppm $^{\bullet}NO_2$ for 30 – 90 min with intermittent cyclic tilting of the glass exposure chamber. DFO was added just prior to exposure onset. Post exposure, RCM were harvested and 3-NT formation assessed via Western analysis as described in Methods. Nitrated BSA was utilized as a positive control standard for 3-NT. As can be seen from this exampled gel ($n \geq 4$ independent RCM preparations and related exposures), under these experimental conditions DFO substantially restricted 3-NT formation for at least 90 min of continuous $^{\bullet}NO_2$ exposure. Also note that the extent of RCM nitration in the absence of DFO increased with exposure time but was extensive (++++) even by the 30 min time point.

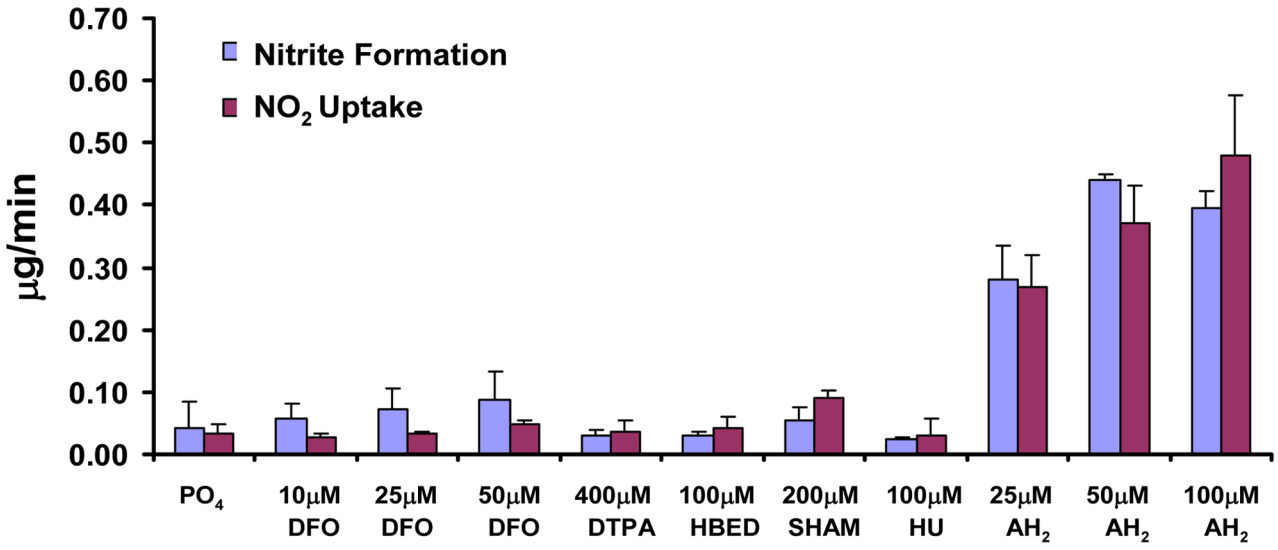

Figure 4. The Extent of $^{\bullet}NO_2$ Uptake and Nitrite Formation across Varying Substrates

As described in methods, solutions at the listed concentrations were exposed under quasi-steady state (with respect to $^{\bullet}NO_2$), well stirred, conditions in small flasks. $^{\bullet}NO_2$ uptake was calculated via the mass balance of gas phase $^{\bullet}NO_2$ across the flasks and the nitrite concentrations determined via the Greiss reaction based on daily standard curves (containing the respective substrate) utilizing $NaNO_2$ as the standard. Data are presented as means +/− one standard deviation of at least 3 independent observations. This approach provides a relative measure of aqueous phase reactivity since the mixing rate, $^{\bullet}NO_2$ delivery rate, and exposure time were all held constant so that differences in uptake and product (nitrite) formation result from the differential driving force for $^{\bullet}NO_2$ interfacial transfer maintained by reaction between solute $^{\bullet}NO_2$ and the substrate of interest. As can be seen, all but the AH_2 showed marginal, if any, uptake rates above the buffer control, suggesting relatively limited reactivity with $^{\bullet}NO_2$. AH_2, which is a well documented facile reactant for $^{\bullet}NO_2$ produced significantly greater rates of uptake and nitrite formation that approximated the 1:1 stoichiometry observed previously. The apparent lack of dose response between 50 and 100 µM likely stemmed for saturation of the interfacial mass transfer rates, which has also been formerly characterized.

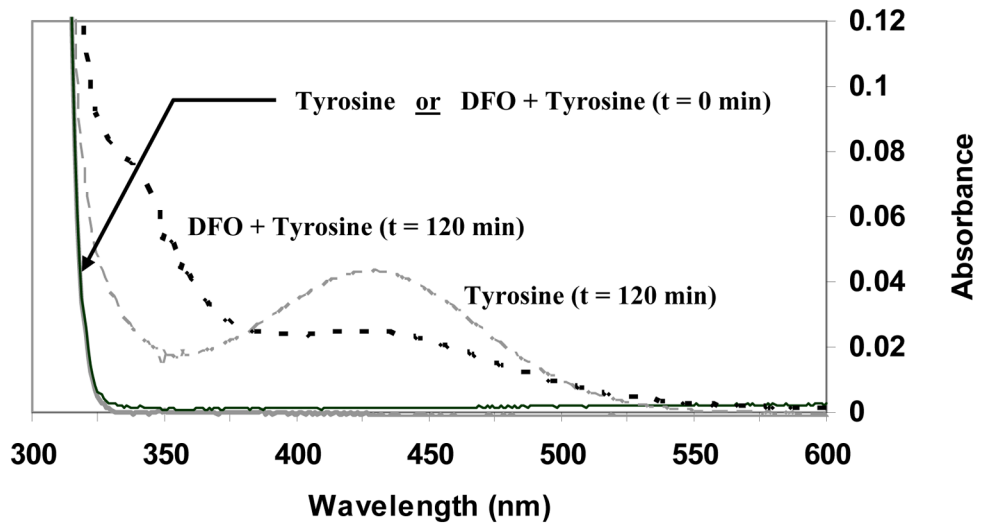

Figure 5. Effect of Desferrioxamine on Aqueous Bulk Phase Tyrosine Nitration

8 ppm $^{\bullet}NO_2$ (mixture of 60 ml/min $^{\bullet}NO_2$ and 520 ml/min air) was bubbled through a 100 ml solution of 0.8 mM tyrosine for 120 min at 25° C. The presence of 3-nitrotyrosine in the solution was measured spectrophotometrically (OD_{438}) at 30 min intervals (long dashed line). At each interval, 2.25 ml of exposed solution were combined with 0.25 ml 1 N NaOH and scanned from 800 – 200 nm. Baseline corrections were made with PO_4 + NaOH solution. Relative to the $^{\bullet}NO_2$ inflow rate, exposed solution volume, tyrosine concentration, and exposure time, the yield of 3-NT based on its alkaline extinction coefficient (~ 4000 M^{-1} cm^{-1}) is within experimental norms. Conditions were then repeated using a 50 μM DFO + 0.8 mM tyrosine solution (short dashed line). Data shown includes t = 0 min and t = 120 min readings. At t = 0 min, spectrophotometric scans of tyrosine and tyrosine + DFO solutions overlie. The addition of DFO to the $^{\bullet}NO_2$ exposed tyrosine markedly reduced 3-NT accumulation.

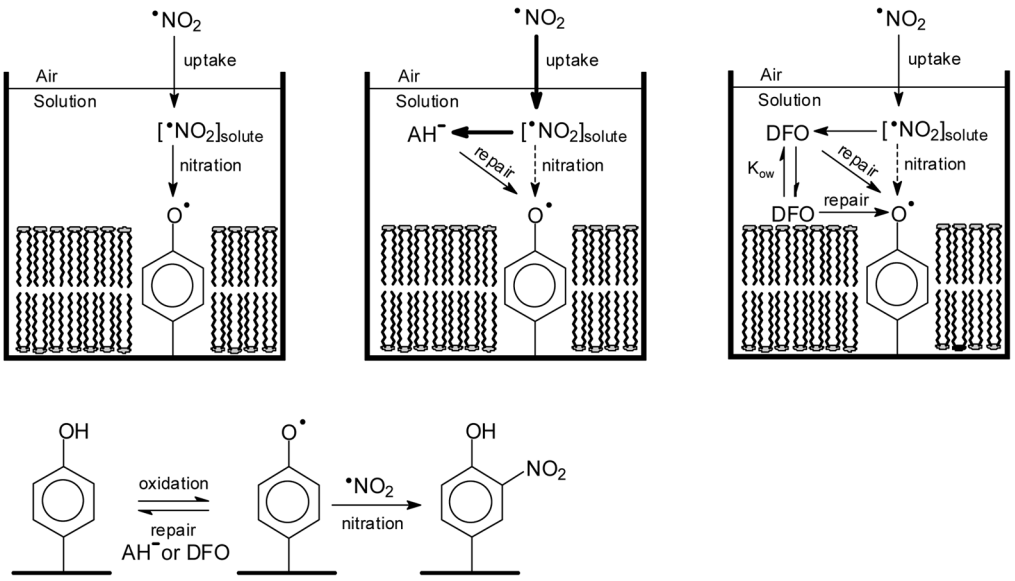

Figure 6. Schematic of the Proposed Differential Mechanisms of Tyrosine Nitration Inhibition

Under conditions similar to the lung surface compartment, reactive uptake of $^{\bullet}NO_2$ may occur by solutions of AH_2 or DFO covering RCM that are chemically bound to the bottom of Petri dishes. At ELF pH (~7.0), essentially all AH_2 will exist as ascorbate (AH^-). This oversimplified cartoon underscores critical differences between these two substrates that result in efficient inhibition of protein tyrosine nitration by DFO as: (1) a larger flux of NO_2 into the AH^- solution, indicated by the bold arrow for NO_2 uptake, that results from the higher reactivity of AH^- for NO_2 (also in bold) as compared to DFO. Notice that the higher reactivity of AH^- facilitates its role as a direct scavenger of NO_2 but also results in faster depletion of AH^-, and (2) the larger log D for DFO that allows for partitioning of DFO into the cell membrane and thereby favors reaction of DFO with inter-membrane tyrosyl radicals while AH^- remains primarily in the aqueous phase which hinders this reaction [log D (DFO) = −3.56; log D (AH^-) = −5.61 at pH 7 (values taken from SciFinder and calculated using Advanced Chemistry Development (ACD/Labs) Software V11.02 (© 1994–2012 ACD/Labs)].

TABLE 1

Influence of Initial Ascorbate Concentrations on $^{\bullet}NO_2$-Induced Membrane Tyrosine Nitration

Aqueous Phase	3-Nitrotyrosine
100 μM AH_2	—
50 μM AH_2	+ + +
25 μM AH_2	+ + +
10 μM AH_2	+ + + +

Red cell membranes (RCM) were covered with differing initial reduced ascorbate (AH_2) concentrations and exposed to 4.5 ppm $^{\bullet}NO_2$ in air for 30 min with cyclic tilting (2 min/side). Following exposure, RCM were washed, membrane proteins isolated, and the presence of 3-nitrotyrosine residues determined by Western analysis. As described in Methods, the extent of 3-NT formation is denoted as extensive (++++), significant (+++), modest (++), little (+), or none (-).

TABLE 2

Influence of Hydroxamic Acids and Related Compounds on $^{\bullet}NO_2$-Induced Membrane Tyrosine Nitration

Aqueous Phase	3-Nitrotyrosine
50 μM DFO	—
200 μM SHA	—
200 μM BHA	+
25 μM Hydroxyurea	+ +
200 μM HBED	+ + +
400 μM DTPA	+ + + +

Red cell membranes (RCM), adhered in petri dishes, were covered with various aqueous phase constituents and exposed to 4.5 ppm $^{\bullet}NO_2$ in air for 30 min with cyclic tilting. Following exposure, RCM were washed, membrane proteins isolated, and the presence of 3-nitrotyrosine residues determined by Western analysis. As described in Methods, the extent of 3-NT formation is denoted as extensive (++++), significant (+++), modest (++), little (+), or none (-). 3-NT was undetectable during air-only exposures.

TABLE 3

Differential Effects of Iron Chelator Pretreatment and Presence during Exposure on $^{\bullet}NO_2$-Induced Membrane Tyrosine Nitration

Pretreatment Chelator	Exposure Aqueous Phase	3-Nitrotyrosine
DTPA	PO_4	+ + + +
DTPA	50 μM DFO	—
DFO	PO_4	+ + + +
DFO	400 μM DTPA	+ + + +

Red cell membranes (RCM), adhered to glass petri dishes, were covered with an aqueous solution containing either 400 μM DTPA or 50 μM DFO. After two 10 min treatments with periodic mixing (gas phase = air), systems were thoroughly rinsed to remove bound Fe complexes and remaining unbound chelator. RCM were then covered with PO_4 buffer alone or buffer + chelator and exposed to 4.5 ppm $^{\bullet}NO_2$ in air for 30 min with cyclic tilting (2 min/side). Following exposure, RCM were washed, membrane proteins isolated, and the presence of 3-nitrotyrosine residues determined by Western analysis. As described in Methods, the extent of 3-NT formation is denoted as extensive (++++), significant (+++), modest (++), little (+), or none (-).

TABLE 4

Effect of Desferrioxamine on Myeloperoxidase-Mediated Membrane Tyrosine Nitration

30 nM MPO	100 μM NO_2^-	100 μM H_2O_2	50 μM DFO	100 μM 4-Aminobenzoic hydrazide	3-Nitrotyrosine
X	X	X	-	-	+ + + +
X	X	-	-	-	—
X	-	X	-	-	—
-	X	X	-	-	—
X	X	X	-	X	—
X	X	X	X	-	—

Adhered red cell membranes (RCM) were covered with 0.7 units/ml myeloperoxidase (MPO) solution, continuously rocked in covered dishes for 15 min, the covering solution removed, and the RCM washed leaving only RCM bound MPO (~ 0.56 units/ml MPO activity). RCM were then covered with various aqueous phase constituents and exposed to air for 30 min with continuous rocking in covered dishes. Following exposure, RCM were washed, membrane proteins isolated and the presence of 3-NT determined by Western analysis. As described in Methods, 3-NT formation is denoted as extensive (+ +++), significant (+++), modest (++), little (+), or none (-).